Generic Role of Polymer Supports in the Fine Adjustment of Interfacial Interactions between Solid Substrates and Model Cell Membranes

Fernanda F. Rossetti,[†,‡] Emanuel Schneck,[†,§] Giovanna Fragneto,[§] Oleg V. Konovalov,[∥] and Motomu Tanaka*,[†,‡]

[†]Physical Chemistry of Biosystems, Physical Chemistry Institute, University of Heidelberg, D-69120 Heidelberg, Germany
[‡]Institute for Integrated Cell-Material Sciences (WPI iCeMS), Kyoto University, 606-8501 Kyoto, Japan
[§]Institut Laue-Langevin (ILL), CS20156, 38042 Grenoble, France
[∥]European Synchrotron Radiation Facility (ESRF), 38042 Grenoble, France

Ⓢ Supporting Information

ABSTRACT: To understand the generic role of soft, hydrated biopolymers in adjusting interfacial interactions at biological interfaces, we designed a defined model of the cell−extracellular matrix contacts based on planar lipid membranes deposited on polymer supports (polymer-supported membranes). Highly uniform polymer supports made out of regenerated cellulose allow for the control of film thickness without changing the surface roughness and without osmotic dehydration. The complementary combination of specular neutron reflectivity and high-energy specular X-ray reflectivity yields the equilibrium membrane−substrate distances, which can quantitatively be modeled by computing the interplay of van der Waals interaction, hydration repulsion, and repulsion caused by the thermal undulation of membranes. The obtained results help to understand the role of a biopolymer in the interfacial interactions of cell membranes from a physical point of view and also open a large potential to generally bridge soft, biological matter and hard inorganic materials.
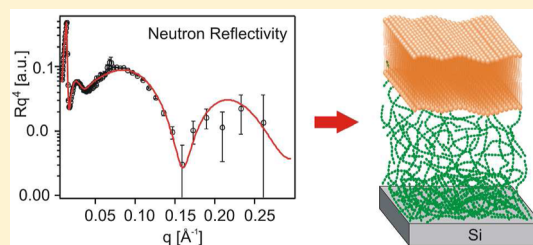
INTRODUCTION

In nature, many contacts between neighboring cell membranes are mediated via hydrated layers of biopolymers, such as glycocalyx and the extracellular matrix. They act as a lubricating layer to avoid nonspecific adhesion and create hydrodynamic pathways for solute transport.

To date, several experimental strategies have been employed to physically model the interfacial interactions in biological systems. Among the simplest model systems of cell membranes are phospholipid bilayers, which are the major component of cell membranes. Specular and off-specular X-ray and neutron scattering of stacks of planar membranes offer a unique advantage over commonly used powder diffraction experiments of lipid suspensions, as the planar geometry of supported membranes enables one to identify in-plane and out-of-plane momentum transfers[1−4] leading to more comprehensive structural data. Information on the structure normal to the sample plane can be obtained from specular scattering, whereas information on the structural ordering parallel to the sample plane (reflecting the mechanical properties of interacting model membranes) can be extracted from off-specular signals.[5−7] As an alternative strategy, Daillant et al. recently proposed the use of specular/off-specular scattering on "floating" phospholipid membranes that are deposited on preformed lipid membranes on planar substrates,[8]

where the off-specular scattering was used to calculate the wall interaction potentials, surface tension, and bending rigidity.

However, in order to understand the interfacial interactions in complex biological systems, it is necessary to create more realistic model systems that allow for highlighting the role of the soft cellular interlayers based on various saccharides. In our previous accounts,[9,10] we utilized oligosaccharide chains coupled to lipid headgroups as a model of the cell surface glycocalyx and demonstrated that the membrane-anchored saccharide chains significantly influence the structure and mechanics of membranes by using specular reflectivity and off-specular scattering.

Another commonly used strategy to physically model interactions mediated via the extracellular matrix is the deposition of lipid membranes on polymer supports. Such systems, called polymer-supported membranes,[11−14] have been proposed as realistic models of biological membranes as they can avoid direct substrate−protein contact and thus the resulting pinning and denaturation of membrane proteins.[15,16] Furthermore, it has been demonstrated that human erythrocyte membranes[17] and sarcoplasmic reticulum membranes can be deposited in an orientation-selective manner using polymer supports based on

Table 1. Thickness, SLD, and Roughness of Dry Cellulose Films as Determined by XRR and NR[a]

	thickness (Å)		SLD (10^{-6} Å^{-2})		roughness (Å)	
	X-ray	neutron	X-ray	neutron	X-ray	neutron
6 layers	40.1 ± 4.5	39 ± 5	7.3 ± 1.5	1.72 ± 0.21	11.1 ± 2.2	20 ± 5
10 layers	41.0 ± 5.8	45 ± 3	11.7 ± 0.6	2.14 ± 0.22	11.3 ± 3.6	18 ± 1
30 layers	130 ± 35	131	12.1 ± 1.1	1.47	18.0 ± 0.1	18

[a]The values are given as the average over several samples ± the standard deviation. For the NR of 30 cellulose layers, no error bars are reported because only 1 sample was used.

regenerated cellulose with a dry thickness of approximately 5 nm. However, in spite of numerous studies utilizing different polymers, including chemically immobilized or cross-linked hydrogels,[18,19] polymer brushes,[20,21] covalently grafted lipo-polymers,[22−24] and polyelectrolyte multilayers,[25,26] there is no quantitative study that highlights how polymer supports would modulate the interfacial interactions.

To resolve the fine structures of polymer-supported membranes at solid/liquid interfaces, specular neutron reflectivity (NR) is one of the straightforward methods. In the 1990s, several groups measured the NR of bilayer lipid membranes directly deposited on solid supports, known as solid-supported membranes.[27,28] However, despite the successful reconstruction of the scattering length density (SLD) profiles, it remained difficult to determine the roughness of lipid membranes in the fluid phase, mainly because of the limited spatial resolution (typically up to q_z = 0.15−0.25 Å^{-1}). The structural characterization of polymer-supported membranes using NR is even more challenging because of the interpenetration of hydrated polymers,[29] formation of incomplete membrane patches,[25] and vague SLD contrast at the polymer/water interface. One of the promising strategies to achieving high spatial resolution to higher q_z is given by specular X-ray reflectivity (XRR) with high-energy X-rays (≥18 keV) that guarantee a high transmittance of X-rays through bulk water.[30,31]

In this work, we determined quantitatively the generic role of polymer supports in the modulation of interfacial interactions by the combination of NR and high-energy XRR. The use of cellulose supports and zwitterionic phosphocholine membranes enabled us to focus on three important interfacial forces, i.e., van der Waals, hydration repulsion, and the thermal undulation force (Helfrich repulsion). The theoretically calculated membrane-substrate distance under equilibrium was validated by the systematic comparison with the experimentally determined membrane−substrate distance for polymer supports with different thicknesses.

MATERIALS AND METHODS

Sample Preparation. Trimethylsilylcellulose (TMSC) was synthesized from cellulose powder (M_w ≈ 25 kDa, purchased from Fluka, Germany), as reported previously.[17,32,33] The average degree of substitution of the three OH groups of the glucose monomers was estimated by elemental analysis to be ~2.1. Two types of silicon substrates were used for the deposition of polymer-supported membranes: (i) one-side-polished silicon [100] wafers with native oxide were purchased from Si-Mat (Landsberg am Lech, Germany), cut into rectangular pieces of 20 × 24 mm^2 and used for X-ray reflectivity and ellipsometry (Plasmos GmbH, Munich, Germany); (ii) single-side-polished (roughness ≈ 5 Å) silicon (111) blocks (80 × 50 × 15 mm^3) coated with native oxide were purchased from Siliciumbearbeitung Holm (Tann, Germany) and used for neutron reflectivity.

Prior to the deposition of cellulose films, the cleaned substrates were hydrophobized by grafting self-assembled monolayers of octadecyl-trimetoxysilane (ODTMS), purchased from ABCR (Karlsruhe, Germany).

Monolayers of TMSC (6, 10, or 30 layers) were transferred from the water surface at a constant surface pressure of 20 mN/m at T = 20 °C with a deposition speed of 4 mm/min and a waiting time of 5 min between layers. Care was taken to always have a transfer ratio greater than 90%. After deposition, the films were exposed to fuming HCl vapor for 10 s. After rinsing with deionized water and drying the samples, we obtained hydrophilic films of regenerated cellulose. It should be noted that films of regenerated cellulose remain stable in organic solvents as well as in aqueous buffers. For XRR measurements, small unilamellar vesicles of 1-stereaoyl-2-oleoyl phosphaphatidylcholine (SOPC, purchased from Avanti Polar Lipids, Alabaster, AL) suspended in phosphate saline buffer (10 mM NaH$_2$PO$_4$, 100 mM NaCl, pH 7.4, employed to simulate physiological conditions) were fused onto polymer supports to form continuous membranes. This was done by incubating the cellulose film with the unilamellar vesicle suspension at 40 °C for at least 1 h and subsequently rinsing away excess vesicles with buffer. For NR experiments, the same procedure was employed, except for the use of a deuterated PBS buffer (10 mM NaH$_2$PO$_4$ and 100 mM NaCl in D$_2$O, pD 7.4) and for longer incubation times of the vesicle suspensions of at least 10 h at 40 °C.

Data Acquisition. High-energy specular X-ray reflectivity experiments were carried out at the ID10B beamline at the European Synchrotron Radiation Facility (ESRF, Grenoble, France). We used specular X-ray reflectivity with high-energy X-ray radiation (21 keV), which guarantees approximately 40% transmission through the 2 cm water path. To exclude the artifacts from radiation damage, we carefully checked the reproducibility of the results by translating the sample position in the direction perpendicular to the beam. Specular neutron reflectivity experiments were carried out in time-of-flight (TOF) mode at the D17 beamline of the Institut Laue Langevin (ILL, Grenoble, France) using D$_2$O instead of H$_2$O.

The specular reflectivity, defined as the ratio between the intensities of reflected and incident beams, was recorded as a function of momentum transfer perpendicular to the membrane plane, q_z = 4π sinα_i/λ, where α_i is the incident angle and λ is the wavelength of the incident beam. For NR, a wavelength range of 2−20 Å was used at two incident angles of 0.8 and 4°. The obtained data were fitted with the programs Motofit[34] and Parratt32.[35] Throughout the fitting of both NR and XRR results, the following constrains were used: (a) the bulk silicon and water parameters of each sample that was measured multiple times (i.e., before and after lipid membrane deposition) were kept constant across all of the data sets; (b) the lowest limit of the root-mean-square (RMS) roughness was kept at 2 Å; (c) membranes were treated as one slab due to the limited spatial resolution of NR; and (d) the roughness at the membrane/water and membrane/cellulose (C2) interfaces was assumed to be conformal.

RESULTS

Dry Cellulose Films Are Molecularly Smooth Irrespective of Total Thickness. Prior to the experiments in aqueous buffer, the polymer supports with 6, 10, and 30 cellulose monolayers were characterized in the dry state by NR and XRR (Supporting Information Figure S1). As summarized in Table 1, both thickness and roughness values show good agreement with ellipsometry results (Supporting Information Table S2) and those in previous accounts,[33,36,37] verifying that the quality of samples is reproducible and independent of the sample size.
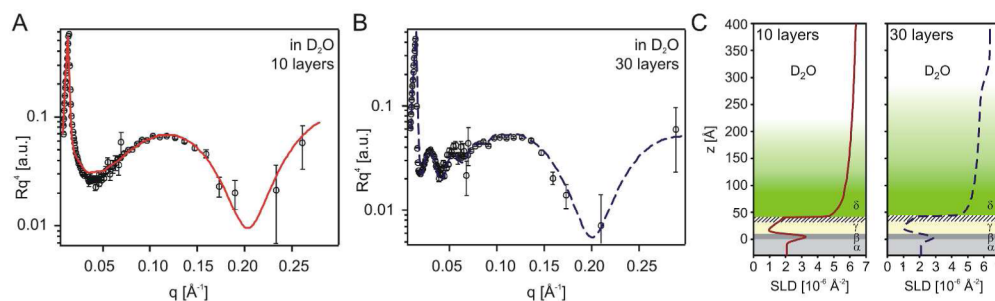
Figure 1. Neutron reflectivity (symbols) and best-fit results (lines) of (A) a thin cellulose film (10 layer) and (B) a thick cellulose film (30 layer) hydrated in PBS (D_2O) buffer and (C) the corresponding SLD profiles along the z axis. α, Si; β, SiO_2; γ, silane; hatched layer, poorly hydrated cellulose (C1); and δ, hydrated cellulose (C2).

The roughness at the cellulose–air interface was below 20 Å for all samples, indicating that the surface roughness value is influenced neither by the total film thickness nor by the size of samples and beam footprints.[36,37] It should be also noted that the film thickness of six cellulose monolayers is about 40–50% larger than that expected from the linear extrapolation of the thickness of 10 and 30 cellulose layers. On the other hand, the corresponding scattering length density (SLD) values are only about 80% (NR) and 60% (XRR) of those of thicker cellulose films (Table 1), suggesting that six layers do not form densely packed films. This effect might be due to the rodlike nature of TMSC, where rods from subsequently deposited layers may fill up defects from the lower layers. Also, the regeneration process of TMSC to cellulose might affect very thin layers differently. (The layer shrinkage for the six-layer samples was only ~40% compared to ~50% for the 10 and 30 layers samples; see Supporting Information Table S2.) Indeed, the average SLDs for thicker films determined from NR and XRR experiments, $b_{nEx} = 2.1 \times 10^{-6}$ Å^{-2} and $b_{eEx} = 11.8 \times 10^{-6}$ Å^{-2}, are in good agreement with those calculated from the bulk density of regenerated cellulose,[38,39] $b_{nCal} = 1.8 \times 10^{-6}$ Å^{-2} and $b_{eCal} = 13.9 \times 10^{-6}$ Å^{-2}, respectively.

Cellulose Films in Water Can Be Represented as "Diffuse" Interfaces. Figure 1A,B represents NR curves for cellulose films with 10 and 30 cellulose monolayers hydrated in bulk PBS (D_2O) buffer, respectively. (The corresponding data obtained by XRR is shown in Supporting Information Figure S3.) In contrast to the reflectivity curves of dry cellulose films in an ambient atmosphere, the reflectivity from the cellulose films in bulk buffer could not be fitted with the standard one-slab model used for dry films. Instead, a two-slab model had to be used, in agreement with earlier studies.[40,41] The first thin cellulose layer adjacent to the hydrophobic alkyl silanes (named the C1 layer, Figure 1C) is poorly hydrated and can be well represented as a slab with a constant SLD and a thickness of 12 ± 4 Å, regardless of the number of cellulose layers. In fact, from the mean SLD, $\langle b_{C1} \rangle = 1.4 \times 10^{-6}$ Å^{-2}, the volume fraction of water in the C1 layer is estimated to be merely 3%. The extremely poor hydration of this layer suggests some interpenetration of cellulose with the hydrophobic silane monolayer, which may also be attributed to the incomplete regeneration of TMSC by HCl vapor treatment. The second layer (named the C2 layer, Figure 1C) shows a much higher degree of hydration than the C1 layer. Its SLD profile cannot be presented as a slab with a distinct thickness and a Gaussian roughness. In order to describe such diffuse interfaces, a commonly used method is to use a roughness parameter to smear out the transition in SLD from one slab to the next.[42−44] However, this is not applicable in our experimental system

because the root-mean-square roughness is comparable to or even larger than the layer thickness. Highly swollen polymer layers at the solid–liquid interface can be fitted either by using a parabolic function[18,45] or by using a stretched exponential function.[10] In this study, we fitted the SLD of the C2 layer with a stretched exponential function, $b(z) = \langle b_{C1} \rangle + (\langle b_{C2} \rangle - \langle b_{C1} \rangle)[1 - e^{-(z/\Lambda)^{2h}}]$, to model the density gradient of polymers in the direction perpendicular to the sample plane, where b_0 is the intrinsic SLD of uniformly hydrated, bulk cellulose, Λ is the characteristic decay length, and h is the stretching exponent. For the thin cellulose layers, we observe how it is not possible to define a clear transition from the hydrated cellulose to the bulk (Figure 1C, left; Supporting Information Figure S3A). However, as the cellulose layers get thicker, the decay is not uniform but an additional distinct density transition appears in the SLD profile (Figure 1C, right; Supporting Information Figure S3B,C) at around 250 Å from the surface. This could indicate the position of the cellulose/bulk interface or a transition within the cellulose layer to a region with even less densely packed cellulose. The results shown below for the membrane-coated samples point to the latter case.

The volume fraction of water in the core of the C2 layer calculated from the mean SLD, $\langle b_{C2} \rangle = (4.6–5.0) \times 10^{-6}$ Å^{-2}, amounts to $\Phi = 0.6–0.7$, which is in contrast to the almost nonhydrated C1 layer. This value agrees very well with the value calculated from film thicknesses measured at low (4%) and high (~98%) relative humidity, corresponding to $\Phi \approx 0.7$.[36] The layer parameters corresponding to the best fit models are summarized in Supporting Information Table S4. The corresponding X-ray reflectivity data, best fit curves, and corresponding layer parameters are presented in Supporting Information Figure S3 and Table S4. The resonant solutions obtained by different SLD contrasts and spatial resolutions demonstrate the robustness and validity of the models.

Fine Structures of Membranes on Polymer Supports. Figure 2A,B represents NR curves (symbols) and the best fit results (solid and dashed lines) of lipid membranes on thin (10 layers) and thick (30 layers) cellulose supports, respectively. The reconstructed SLD profiles and the schematic illustrations of the systems are shown in Figure 2C. In contrast to the diffuse interface observed at the cellulose/water interface, the membrane/cellulose interface and the membrane/water interface are more distinctly highlighted because of the hydrocarbon chains of the lipid membrane.[29] Despite the poor statistics at $q_z \geq 0.2$ Å^{-1}, the clearer SLD contrast between lipid membranes ($\langle b_{lipid} \rangle = 3.6 \times 10^{-6}$ Å^{-2}) and the two neighboring layers ($\langle b_{C2} \rangle = 5.4 \times 10^{-6}$ Å^{-2}, $\langle b_{D_2O} \rangle = 6.4 \times 10^{-6}$ Å^{-2}) enables one to distinguish the C2 layer as a "slab".
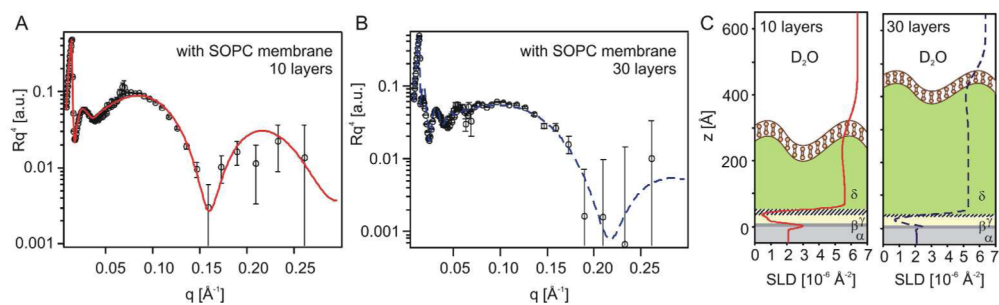
Figure 2. Neutron reflectivity (symbols) and best fit results (lines) of SOPC membranes deposited on (A) a thin (10 layer) and (B) a thick (30 layer) cellulose support and (C) the corresponding SLD profiles. Note that the C2 layer (δ) can be well fitted as a slab in the presence of membranes. α, Si; β, SiO$_2$; γ, silane; hatched layer, poorly hydrated cellulose (C1); and δ, hydrated cellulose (C2).
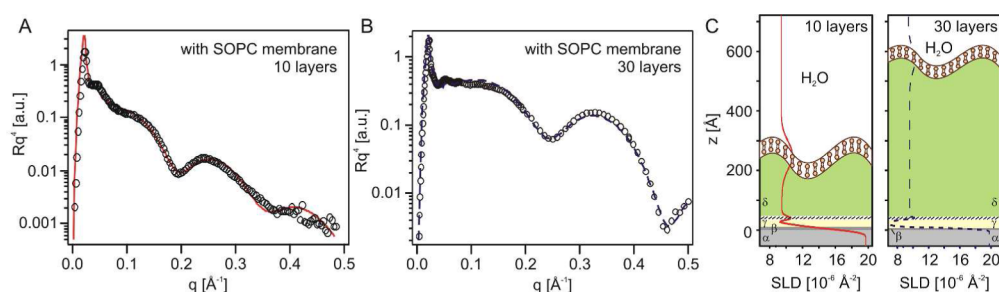
Figure 3. High-energy X-ray reflectivity (symbols) and the best fit results (lines) of SOPC membranes deposited on (A) a thin (10 layers) and (B) a thick (30 layer) cellulose support and (C) the corresponding SLD profiles. Note that the best fit models from XRR and NR are consistent despite the different spatial resolution, sample size, and SLD contrasts (Table 2). α, Si; β, SiO$_2$; γ, silane; hatched layer, poorly hydrated cellulose (C1); and δ, hydrated cellulose (C2).

Table 2. Layer Parameters Obtained from the Best Fits of NR and XRR Results for Lipid Membranes on Thin (10 Layer) and Thick (30 Layer) Cellulose Supports[a]

	thickness (Å)		SLD (10^{-6} Å^{-2})		roughness (Å)	
NR	10 layers	30 layers	10 layers	30 layers	10 layers	30 layers
D$_2$O			6.366	6.366	73 ± 11	50
SOPC	34 ± 3	33	3.31 ± 0.47	3.75	73 ± 11	50
C2	173 ± 24	378	5.51 ± 0.09	5.29	8.1 ± 1.6	7.0
C1	16 ± 3	8	1.28 ± 0.96	1.58	6.3 ± 1.7	8.8
	thickness (Å)		SLD (10^{-6} Å^{-2})		roughness (Å)	
XRR	10 layers	30 layers	10 layers	30 layers	10 layers	30 layers
D$_2$O			9.41	9.41	52 ± 6	65
SOPC	36 ± 2	35	15.1 ± 1.1	13.9	52 ± 6	65
C2	189 ± 8	455	9.93 ± 0.75	9.51	6.6 ± 2.9	4.7
C1	9 ± 2	10	11.4 ± 0.5	11.4	6.5 ± 2.3	3.0

[a]All samples were characterized before and after deposition of the membrane (same sample). For each individual sample, the parameters from the layers below (silane, SiO$_2$, and Si) were kept the same as before the deposition of the membrane (data shown in Supporting Information Table S4). In all cases, the fit gave the same picture, i.e., the presence of a 3- to 4-nm-thick membrane with a very high "roughness" of 5−8 nm, attributable to undulation. For a discussion of the most important model parameters (thickness of the hydrated cellulose C2, membrane roughness), see Supporting Information S8. The values are given as the average over several samples ± the standard deviation. For the NR of 30 cellulose layers, no error bars are reported because only one sample was used.

It is interesting that the thickness of the C2 layer for the thicker, 30-layer cellulose (378 Å for NR and 455 Å for XRR) is much larger than the distance between the C1 layer and the transition region observed in the SLD profiles in Figure 1C(right) and Supporting Information Figure 3C (~250 and ~300 Å, respectively). This indicates that the cellulose/bulk interface is not as well defined as the SLD profiles would lead us to think but that this transition region reaches much further into the bulk, even if it cannot be observed due to the lack of contrast. To determine if the amount of cellulose is conserved, we calculated the z-integrated reduction in SLD with respect to pure D$_2$O, before and after

membrane deposition for the same sample with 30 layers of cellulose. We obtained 1.70×10^{-4} Å^{-2}nm before membrane deposition and 3.47×10^{-4} Å^{-2} nm after. The fact that the amount of cellulose detected after membrane deposition is higher than before supports the above assumption.

It is noteworthy that the same layer models can well represent the XRR results up to a higher momentum transfer of $q_z = 0.5$ Å^{-1} (Figure 3A,B). As summarized in Table 2, both the thickness and roughness of each layer are in satisfactory agreement between NR and XRR measurements despite the different SLD contrasts and spatial resolutions (Figures 2C and 3C). Deviations can be

attributed to slightly different structural characteristics between samples prepared for NR and XRR (e.g., due to the different sample size). The best-fit results of NR and XRR curves also indicate that the membrane/water and thus membrane/C2 interfaces have a relatively high RMS roughness of $\sigma = 50-70$ Å. Because a lipid membrane has an essentially constant thickness, a given roughness on one surface must be accompanied by approximately the same roughness on the other surface. This roughness is attributable to the undulations of the membrane averaged over time, as discussed in the next paragraph. The relatively high neutron SLD value of the lipid membrane may indicate an incomplete coverage of the surface, with defects in the membrane filled with D_2O, even though it is difficult to interpret this number in view of the high RMS roughness. We demonstrated in a previous account[15] that the deposition of lipid membranes on cellulose cushions reproducibly leads to a fully covered surface (Supporting Information Figure S5). However, the substrates used for NR have a very large surface (40 cm^2), which may increase the likelihood of defects in the lipid membrane.

In general, a larger roughness would reflect the shallower confinement of interaction potentials between membranes and substrates. For example, lipid membranes directly deposited on solid supports are sharply confined in the proximity of the substrate (typical membrane–substrate distance of about 0.5 nm[30,46]) by dominant van der Waals interactions. Here, the membrane roughness reflects the roughness of the underlying substrate. The RMS roughness values of solid-supported membranes in the gel and fluid phases as determined by NR[27] and XRR[30] are in the range of $\sigma = 4-7$ Å, which seems to be in good agreement with substrate roughness. On the other hand, the insertion of additional "spacer" layers would lead to a shallower confinement of interfacial interaction potentials, which results in a more pronounced fluctuation and thus a larger roughness. For example, Charitat et al. deposited another lipid membrane on a predeposited solid-supported membrane and reported that the distal membrane possesses an RMS roughness of $\sigma = 13$ Å, much larger than that of the proximal membrane ($\sigma = 7$ Å), although the membranes are separated by only 20 Å. This finding corroborates our interpretation of thermal membrane fluctuations as a major contribution to membrane roughness.[27] Previously, Wong et al. deposited phosphatidyl choline membranes on "dry" polyethylenimine and reported an RMS roughness of $\sigma = 6$ Å,[26] whereas Majewski and co-workers reported an RMS roughness of $\sigma = 105$ Å for a DPPC membrane deposited on a swollen poly(*N*-isopropylacrylamide) copolymer.[47] Such a large difference in the measured roughnesses for dry and highly swollen polymers suggests that membranes deposited on the latter substrates no longer follow the topography of the underlying layer but rather that there is a substantial contribution of thermal undulations. To validate our slab model with a large RMS roughness obtained by fitting, the experimental results were also simulated by slicing the SLD profile into 200 slabs of 2 Å with roughness $\sigma = 0$.[48] As presented in Supporting Information Figure S6, the deviation between the two curves has a negligible influence on the fit quality. Therefore, our experimental finding can be qualitatively interpreted in terms of a soft, hydrated cellulose support which simultaneously introduces additional cellulose–membrane interactions.

Interplay of Interfacial Forces Determines the Equilibrium Membrane–Substrate Distance. In general, the interactions of lipid membranes and solid substrates can be described as an interaction between two planes via a thin interlayer. Derjaguin described the thermodynamics of thin liquid films by using the concept of a disjoining pressure Π, which is the sum of the various interfacial forces.[47,49] Because the increase in the Gibbs free energy due to the change in the interplane distance is related to the disjoining pressure

$$G = -\int_D^\infty \Pi(D')\, dD' \tag{1}$$

a stable, finite separation distance under thermodynamic equilibrium should fulfill $\Pi(D) = 0$. Thus, in order to better understand the interplay of interfacial forces in the fine adjustment of membrane–substrate interactions, we calculated disjoining pressures by taking three major force contributors into account: (a) the van der Waals force, (b) hydration repulsion, and (c) undulation repulsion originating from the thermodynamic fluctuation of the membrane [Our experimental system consists of a neutral polysaccharide (cellulose) and zwitterionic phosphatidylcholine (SOPC). Throughout this study, we used phosphate buffers with 100 mM NaCl. Because the Debye screening length in the buffer (<10 Å) is more than 1 order of magnitude smaller than the thickness of the polymer supports, we did not include electrostatic interactions in our force calculations.]

First, the van der Waals force is calculated by using an asymmetric five-layer model:[50]

$$P_{\text{vdW}} = \frac{1}{6\pi}\left[\frac{A_{234}}{D^3} - \frac{\sqrt{A_{121}A_{343}}}{(D+T_2)^3} - \frac{\sqrt{A_{545}A_{323}}}{(D+T_4)^3} + \frac{\sqrt{A_{545}A_{121}}}{(D+T_2+T_4)^3}\right] \tag{2}$$

As depicted in Figure 4A, A_{ijk} is the Hamaker constant corresponding to the interaction between media i and k across medium j (Table 3), T_2 the thickness of the lipid membrane (on average, 34.6 Å), T_4 is the sum of the thickness of C1 and silane layers (average 36.0 Å), and D is the thickness of the hydrated C2 layer. Details about the choice of the Hamaker constants are described in Supporting Information S7.

Second, hydration repulsion originates from the work necessary to remove water from a hydrated layer to the infinitely thick bulk liquid phase, and thus $P_{\text{hyd}}(D)$ can be represented by an exponential decay function:[51,52]

$$P_{\text{hyd}} = P_0 \exp\left[-C\left(\frac{D}{D_0}\right)\right] \tag{3}$$

P_0 is an intrinsic pressure, D/D_0 is the ratio between the thickness of hydrated and dry films, and C is a characteristic constant. $P_0 = 5.81 \times 10^{10}$ Pa and $C = 6.24$ were determined experimentally by measuring the equilibrium thickness of identically prepared cellulose films under different osmotic pressures at room temperature, as described previously.[36]

Third, the repulsive pressure caused by the thermal undulation of membranes, called Helfrich repulsion,[53,54] can be given as

$$P_{\text{und}}(D) = \alpha_1 \frac{(k_B T)^2}{\kappa D^3} \tag{4}$$

for a single supported membrane fluctuating next to the wall. κ is the bending rigidity of the membrane ($\sim 10kT$). The hydrated cellulose layer of thickness D is treated as fully membrane-
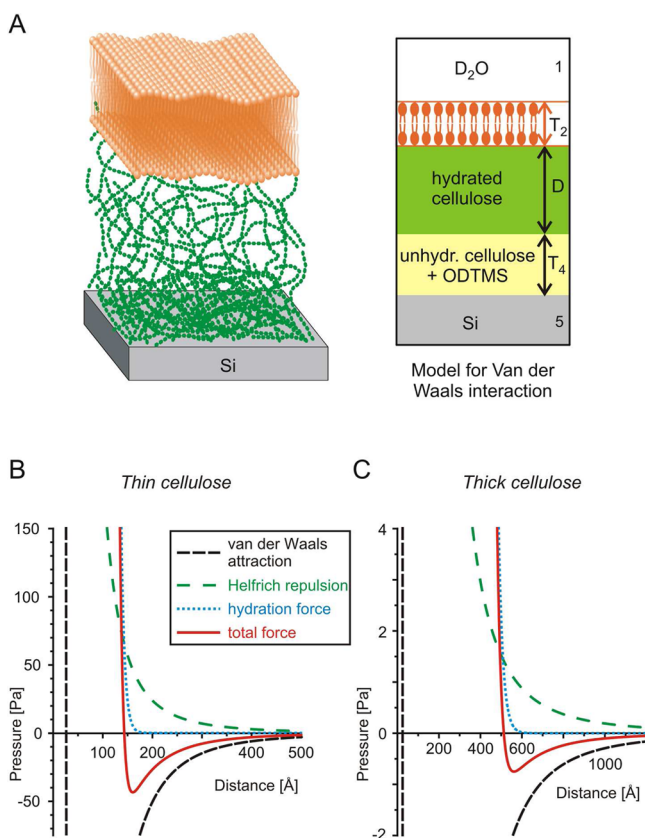
Figure 4. (A) Schematic illustration of a polymer-supported membrane (left) and the asymmetric five-layer model used for the calculation of interfacial forces (right). (B, C) Interfacial forces plotted as a function of the thickness of C2 (D) for (B) thin (10 layer) and (C) thick (30 layer) cellulose supports: van der Waals force (black), hydration repulsion (blue), Helfrich repulsion (green), and the sum of three forces (disjoining pressure, red).

Table 3. Hamaker Constants Used for the Calculation of P_{vdW}[a]

interaction	symbol	value (J)
SLM/C2/HC	A_{234}	2.0×10^{-21}
w/SLM/w	A_{121}	8.0×10^{-21}
C2/HC/C2	A_{343}	7.0×10^{-21}
Si/HC/Si	A_{545}	111.6×10^{-21}
C2/SLM/C2	A_{323}	7.0×10^{-21}

[a]The numerical indices of the symbols correspond to the layer numbers in Figure 4A. SLM, supported lipid membrane; HC, silane + C1; w, water; Si, silicon.

permeable, so eq 4 can be understood as a lower estimate of the Helfrich repulsion. The prefactor, $\alpha_1 = (\pi^2/128)$, has been found by analytical derivation and was confirmed by Monte Carlo simulations.[54] As shown further below, the Helfrich repulsion makes a minor contribution to the interfacial force balance.

Figure 4 represents the van der Waals force (black), hydration repulsion (blue), and Helfrich repulsion (green) plotted as a function of D, i.e., the thickness of C2. The sum of three forces, i.e., the disjoining pressure,

$$\Pi = P_{vdW} + P_{hyd} + P_{und} \qquad (5)$$

is given in red for thin and thick cellulose layers. In the case of a thin cellulose support (10 layers, Figure 4B), the predicted

disjoining pressure has a distinct point of zero force at $D_{eq\_thin} = 142$ Å. This value is in satisfactory agreement with the results from NR and XRR measurements $D_{NR} \approx 170$ Å and $D_{XRR} \approx 190$ Å if one considers the approximations and assumptions that needed to be introduced for estimating the Hamaker constants. Additionally, it should be noted that for calculating the van der Waals interactions some of the slabs of our actual seven-layer system were combined to obtain the five-layer model shown in Figure 4, thus introducing further uncertainties. The point of zero force and the corresponding equilibrium distance for the thick cellulose support (30 layers, Figure 4C) are much more vaguely defined at around $D_{eq\_thick} = 513$ Å but are also in the same range as the experimental results, $D_{NR} \approx 380$ Å and $D_{XRR} \approx 460$ Å.

■ DISCUSSION

Leibler and Lipowsky[55] theoretically described a continuous unbinding transition between neighboring membranes in three-dimensional space by varying the intermembrane spacing, suggesting that such a transition should be detected experimentally. Marx et al.[56] prepared giant vesicles incorporating lipids with poly(ethylene glycol) (PEG) headgroups and cholesterol and monitored the fluctuation of the membranes on a surface passivated with nonfat dry milk using microinterferometry. They observed that the probability functions of the membrane−substrate distance of multicomponent vesicles show double Gaussian peaks, suggesting that (a) the collision of multicomponent membranes induces phase separation[57] and (b) the unbinding transition is a first-order transition.[58,59]

Within the theoretical framework of Leibler and Lipowsky,[55] the fluctuation amplitude of unbound membranes $\phi(\vec{r}, t) = D(h, t) - \langle D \rangle$ is governed by a Gaussian Hamiltonian:

$$H[\phi] = \frac{1}{2}\kappa \int d^2r [(\nabla^2\phi)^2 + 4\xi_\parallel^{-4}\phi^2] \qquad (6)$$

$\xi_\parallel$ is the lateral fluctuation wavelength, and κ is the bending rigidity of the membrane. The RMS width of the probability function derived from the above equation is $(\langle\phi^2\rangle)^{1/2} = \langle D \rangle / C_\perp$, where $C_\perp = 5^{1/2}$ is a universal amplitude ratio.[57] In fact, Netz et al.[57] showed that the RMS width/roughness of the fluctuation amplitude of single-component lipid vesicles (no cholesterol, no PEG lipids) hovering over the passive substrate at a distance of $\langle D \rangle \approx 500$ Å was ~250 Å, which is close to the theoretical prediction. In contrast, the RMS roughness values, $\sigma = 50-70$ Å, that we obtained by NR and XRR for the polymer-supported membranes at distances in the range of $D \approx 170-460$ Å from the solid surface do not linearly scale with $\langle D \rangle$ and are smaller than the ones predicted for a noninteracting spacer layer, $\sigma \approx \langle D \rangle / 5^{1/2} \approx 80-200$ Å. This damping suggests that polymer supports do not merely act as a water reservoir that fills the membrane−substrate gap but rather that the membrane is coupled to the underlying cellulose layer to a certain extent so that the membrane is not physically decoupled from the surface.

As presented in Figure 4, the disjoining pressures in both systems are dominated by the interplay of the attractive van der Waals force and hydration repulsion whereas the Helfrich repulsion, due to its shallower slope, makes a smaller contribution (for instance, increasing the temperature to 60 °C would increase D_{eq_thin} to only 144 Å and D_{eq_thick} to only 521 Å) and is not sufficient to physically decouple the membrane from the surface due to the thermal fluctuation. The latter may occur when the polymer supports become very thick and/or highly hydrated, as seems to be consistent with the previous work reporting the

decoupling (budding) of supported membranes on highly swollen dextran supports (swollen by a factor of 100−150).[19,60] Because interfacial interactions in biological systems include various charged molecular components, such as cell surface glycocalyx and glycosaminoglycans, experiments with charged polymer supports and charged membranes would help us gain deeper insight into the contribution of electrostatic interactions at soft biological interfaces. Moreover, polymer-supported membranes not only serve as a defined model of biological interfaces but also can be utilized to bridge soft biological matter and inorganic materials such as semiconductors.[11,12] The quantitative understanding of the interplay of interfacial interactions by soft interlayers would allow for the rational design of polymeric materials for the fabrication of bioinorganic composite materials.

■ ASSOCIATED CONTENT

Ⓢ Supporting Information

Neutron and X-ray reflectivity curves for dry cellulose samples of different thickness. Film thickness of the dry cellulose films obtained by ellipsometry. X-ray reflectivity of hydrated cellulose films. Parameters used for fitting the hydrated cellulose samples. Images of an SOPC membrane deposited on a cellulose support. Comparison between the fitting curve based on the slab model and the simulated reflectivity data. Hamaker constants. This material is available free of charge via the Internet at http://pubs.acs.org

■ AUTHOR INFORMATION

Corresponding Author
*E-mail: tanaka@uni-heidelberg.de.
Notes
The authors declare no competing financial interest.

■ ACKNOWLEDGMENTS

■ REFERENCES

(1) Safinya, C. R.; Sirota, E. B.; Roux, D.; Smith, G. S. Universality in Interacting Membranes - the Effect of Cosurfactants on the Interfacial Rigidity. *Phys. Rev. Lett.* **1989**, *62*, 1134−1137.

(2) Salditt, T. Structure and fluctuations of highly oriented phospholipid membranes. *Curr. Opin. Colloid Interface Sci.* **2000**, *5*, 19−26.

(3) Katsaras, J. Highly aligned lipid membrane systems in the physiologically relevant "excess water" condition. *Biophys. J.* **1997**, *73*, 2924−2929.

(4) Liu, Y.; Nagle, J. F. Diffuse scattering provides material parameters and electron density profiles of biomembranes. *Phys. Rev. E* **2004**, *69*, 040901.

(5) Pabst, G.; Katsaras, J.; Raghunathan, V. A.; Rappolt, M. Structure and Interactions in the Anomalous Swelling Regime of Phospholipid Bilayers. *Langmuir* **2003**, *19*, 1716−1722.

(6) Salditt, T. Thermal fluctuations and stability of solid-supported lipid membranes. *J. Phys.: Condens. Matter* **2005**, *17*, R287−R314.

(7) Yamada, N. L.; Seto, H.; Takeda, T.; Naga, M.; Kawabata, Y.; Inoue, K. SAXS, SANS and NSE studies on "unbound state" in DPPC/water/CaCl2 system. *J. Phys. Soc. Jpn.* **2005**, *74*, 2853−2859.

(8) Daillant, J.; Bellet-Amalric, E.; Braslau, A.; Charitat, T.; Fragneto, G.; Graner, F.; Mora, S.; Rieutord, F.; Stidder, B. Structure and fluctuations of a single floating lipid bilayer. *Proc. Natl. Acad. Sci. U.S.A.* **2005**, *102*, 11639−11644.

(9) Schneck, E.; Oliveira, R. G.; Rehfeldt, F.; Deme, B.; Brandenburg, K.; Seydel, U.; Tanaka, M. Mechanical properties of interacting lipopolysaccharide membranes from bacteria mutants studied by specular and off-specular neutron scattering. *Phys. Rev. E* **2009**, *80*, 041929.

(10) Schneck, E.; Papp-Szabo, E.; Quinn, B. E.; Konovalov, O. V.; Beveridge, T. J.; Pink, D. A.; Tanaka, M. Calcium ions induce collapse of charged O-side chains of lipopolysaccharides from Pseudomonas aeruginosa. *J. R. Soc., Interface* **2009**, *6*, S671−S678.

(11) Tanaka, M.; Sackmann, E. Polymer-Supported Membranes as Models of the Cell Surface. *Nature* **2005**, *437*, 656−663.

(12) Tanaka, M. Polymer-supported membranes: Physical models of cell surfaces. *MRS Bull.* **2006**, *31*, 513−520.

(13) Beyer, D.; Elender, G.; Knoll, W.; Kühner, M.; Maus, S.; Ringsdorf, H.; Sackmann, E. Influence of Anchor Lipids on the Homogeneity and Mobility of Lipid Bilayers on Thin Polymer Films. *Angew. Chem., Int. Ed. Engl.* **1996**, *35*, 1682−1685.

(14) Cassier, T.; Sinner, A.; Offenhäuser, A.; Möhwald, H. Homogeneity, electrical resistivity and lateral diffusion of lipid bilayers coupled to polyelectrolyte multilayers. *Colloids Surf., B* **1999**, *15*, 215−225.

(15) Goennenwein, S.; Tanaka, M.; Hu, B.; Moroder, L.; Sackmann, E. Functional incorporation of integrins into solid supported membranes on ultrathin films of cellulose: Impact on adhesion. *Biophys. J.* **2003**, *85*, 646−655.

(16) Tutus, M.; Rossetti, F. F.; Schneck, E.; Fragneto, G.; Forster, F.; Richter, R.; Nawroth, T.; Tanaka, M. Orientation-Selective Incorporation of Transmembrane F0F1 ATP Synthase Complex from Micrococcus luteus in Polymer-Supported Membranes. *Macromol. Biosci.* **2008**, *8*, 1034−1043.

(17) Tanaka, M.; Kaufmann, S.; Nissen, J.; Hochrein, M. Orientation selective immobilization of human erythrocyte membranes on ultrathin cellulose films. *Phys. Chem. Chem. Phys.* **2001**, *3*, 4091−4095.

(18) Kuhl, T. L.; Majewski, J.; Wong, J. Y.; Steinberg, S.; Leckband, D. E.; Israelachvili, J. N.; Smith, G. S. A neutron reflectivity study of polymer-modified phospholipid monolayers at the solid-solution interface: Polyethylene glycol-lipids on silane-modified substrates. *Biophys. J.* **1998**, *75*, 2352−2362.

(19) Kühner, M.; Tampé, R.; Sackmann, E. Lipid mono- and bilayer supported on polymer films: Composite polymer-lipid films on solid substrates. *Biophys. J.* **1994**, *67*, 217−226.

(20) Rehfeldt, F.; Steitz, R.; Armes, S. P.; von Klitzing, R.; Gast, A. P.; Tanaka, M. Reversible activation of diblock copolymer monolayers at the interface by pH modulation, 2: Membrane interactions at the solid/liquid interface. *J. Phys. Chem. B* **2006**, *110*, 9177−9182.

(21) Kaufmann, S.; Borisov, O.; Textor, M.; Reimhult, E. Mechanical properties of mushroom and brush poly(ethylene glycol)-phospholipid membranes. *Soft Matter* **2011**, *7*, 9267−9275.

(22) Naumann, C. A.; Prucker, O.; Lehmann, T.; Rühe, J.; Knoll, W.; Frank, C. W. The Polymer-Supported Phospholipid Bilayer: Tethering as a New Approach to Substrate-Membrane Stabilization. *Biomacromolecules* **2001**, *3*, 27−35.

(23) Purrucker, O.; Förtig, A.; Jordan, R.; Tanaka, M. Supported Membranes with Well-Defined Polymer Tethers - Incorporation of Cell Receptors. *ChemPhysChem* **2004**, *5*, 327−335.

(24) Wagner, M. L.; Tamm, L. K. Tethered Polymer-Supported Planar Lipid Bilayers for Reconstitution of Integral Membrane Proteins: Silane-Polyethyleneglycol-Lipid as a Cushion and Covalent Linker. *Biophys. J.* **2000**, *79*, 1400−1414.

(25) Delajon, C.; Gutberlet, T.; Steitz, R.; Mohwald, H.; Krastev, R. Formation of polyelectrolyte multilayer architectures with embedded DMPC studied in situ by neutron reflectometry. *Langmuir* **2005**, *21*, 8509−8514.

(26) Wong, J. Y.; Majewski, J.; Seitz, M.; Park, C. K.; Israelachvili, J. N.; Smith, G. S. Polymer-cushioned bilayers. I. A structural study of various preparation methods using neutron reflectometry. *Biophys. J.* **1999**, *77*, 1445−1457.

(27) Charitat, T.; Bellet-Amalric, E.; Fragneto, G.; Graner, F. Adsorbed and free lipid bilayers at the solid-liquid interface. *Eur. Phys. J. B* **1999**, *8*, 583−593.

(28) Koenig, B. W.; Krueger, S.; Orts, W. J.; Majkrzak, C. F.; Berk, N. F.; Silverton, J. V.; Gawrisch, K. Neutron Reflectivity and Atomic Force Microscopy Studies of a Lipid Bilayer in Water Adsorbed to the Surface of a Silicon Single Crystal. *Langmuir* **1996**, *12*, 1343−1350.

(29) Majewski, J.; Wong, J. Y.; Park, C. K.; Seitz, M.; Israelachvili, J. N.; Smith, G. S. Structural studies of polymer-cushioned lipid bilayers. *Biophys. J.* **1998**, *75*, 2363−2367.

(30) Miller, C. E.; Majewski, J.; Gog, T.; Kuhl, T. L. Characterization of biological thin films at the solid-liquid interface by x-ray reflectivity. *Phys. Rev. Lett.* **2005**, *94*, 238104.

(31) Seitz, P. C.; Reif, M. D.; Konovalov, O. V.; Jordan, R.; Tanaka, M. Modulation of substrate-membrane interactions by linear poly(2-methyl-2-oxazoline) spacers revealed by X-ray reflectivity and ellipsometry. *ChemPhysChem* **2009**, *10*, 2876−83.

(32) Klebe, J. F.; Finkbeiner, H. L. Silyl celluloses: A new class of soluble cellulose derivatives. *J. Polym. Sci., Part A-1: Polym. Chem.* **1969**, *7*, 1947−1958.

(33) Schaub, M.; Wenz, G.; Wegner, G.; Stein, A.; Klemm, D. Ultrathin Films of Cellulose on Silicon-Wafers. *Adv. Mater.* **1993**, *5*, 919−922.

(34) Nelson, A. Co-refinement of multiple-contrast neutron/X-ray reflectivity data using MOTOFIT. *J. Appl. Crystallogr.* **2006**, *39*, 273−276.

(35) Parratt, L. G. Surface Studies of Solids by Total Reflection of X-Rays. *Phys. Rev.* **1954**, *95*, 359.

(36) Rehfeldt, F.; Tanaka, M. Hydration Forces in Ultrathin Films of Cellulose. *Langmuir* **2003**, *19*, 1467−1473.

(37) Rossetti, F. F.; Panagiotou, P.; Rehfeldt, F.; Schneck, E.; Dommach, M.; Funari, S. S.; Timmann, A.; Mueller-Buschbaum, P.; Tanaka, M. Structures of regenerated cellulose films revealed by grazing incidence small-angle x-ray scattering. *Biointerphases* **2008**, *3*, 117−127.

(38) Segal, L.; Creely, J. J.; Martin, A. E.; Conrad, C. M. An Empirical Method for Estimating the Degree of Crystallinity of Native Cellulose Using the X-Ray Diffractometer. *Text. Res. J.* **1959**, *29*, 786−794.

(39) Sparke, E. J. The preparation of continuous filament yarns for weaving and knitting. The effects of denier, elongation and strength on the behaviour of twisted singles yarn. *J. Text. Inst. Proc.* **1950**, *41*, P69−P78.

(40) Penfold, J.; Tucker, I.; Petkov, J.; Thomas, R. K. Surfactant Adsorption onto Cellulose Surfaces. *Langmuir* **2007**, *23*, 8357−8364.

(41) Tucker, I.; Petkov, J.; Penfold, J.; Thomas, R. K. Adsorption of Nonionic and Mixed Nonionic/Cationic Surfactants onto Hydrophilic and Hydrophobic Cellulose Thin Films. *Langmuir* **2010**, *26*, 8036−8048.

(42) Doshi, D. A.; Watkins, E. B.; Israelachvili, J. N.; Majewski, J. Reduced water density at hydrophobic surfaces: Effect of dissolved gases. *Proc. Natl. Acad. Sci. U.S.A.* **2005**, *102*, 9458−9462.

(43) Tidswell, I. M.; Ocko, B. M.; Pershan, P. S.; Wasserman, S. R.; Whitesides, G. M.; Axe, J. D. X-ray specular reflection studies of silicon coated by organic monolayers (alkylsiloxanes). *Phys. Rev. B* **1990**, *41*, 1111−1128.

(44) Charitat, T.; Lecuyer, S.; Fragneto, G. Fluctuations and destabilization of single phospholipid bilayers. *Biointerphases* **2008**, *3*, FB3−FB15.

(45) Milner, S. T.; Witten, T. A.; Cates, M. E. Theory of the Grafted Polymer Brush. *Macromolecules* **1988**, *21*, 2610−2619.

(46) Nováková, E.; Giewekemeyer, K.; Salditt, T. Structure of two-component lipid membranes on solid support: An X-ray reflectivity study. *Phys. Rev. E* **2006**, *74*, 051911.

(47) Smith, H. L.; Jablin, M. S.; Vidyasagar, A.; Saiz, J.; Watkins, E.; Toomey, R.; Hurd, A. J.; Majewski, J. Model Lipid Membranes on a Tunable Polymer Cushion. *Phys. Rev. Lett.* **2009**, *102*, 228102.

(48) Nevot, L.; Croce, P. Characterization of surfaces by grazing x-ray reflection - application to study of polishing of some silicate-glasses. *Rev. Phys. Appl.* **1980**, *15*, 761−779.

(49) Derjaguin, B. V.; Churaev, N. V. *Surface Forces*; Consultants Bureau: New York, 1987.

(50) Israelachvili, J. N. *Intermolecular and Surface Forces*, 2nd ed.; Academic Press: London, 1992.

(51) Rau, D. C.; Parsegian, V. A. Direct measurement of forces between linear polysaccharides xanthan and schizophyllan. *Science* **1990**, *249*, 1278−1281.

(52) Leikin, S.; Parsegian, V. A.; Rau, D. C.; Rand, R. P. Hydration Forces. *Annu. Rev. Phys. Chem.* **1993**, *44*, 369−395.

(53) Helfrich, W. Steric interaction of fluid membranes in multilayer systems. *Z. Naturforsch., A* **1978**, *33*, 305−315.

(54) Bachmann, M.; Kleinert, H.; Pelster, A. Fluctuation pressure of a stack of membranes. *Phys. Rev. E* **2001**, *63*, 051709.

(55) Leibler, S.; Lipowsky, R. Extreme swelling of lamellar phases. *Phys. Rev. Lett.* **1987**, *58*, 1796−1796.

(56) Marx, S.; Schilling, J.; Sackmann, E.; Bruinsma, R. F. Helfrich Repulsion and Dynamical Phase Separation of Multicomponent Lipid Bilayers. *Phys. Rev. Lett.* **2002**, *88*, 138102.

(57) Netz, R. R.; Pincus, P. Inhomogeneous fluid membranes - segregation, ordering, and effective rigidity. *Phys. Rev. E* **1995**, *52*, 4114−4128.

(58) Bruinsma, R.; Sackmann, E. Bioadhesion and the dewetting transition. *C. R. Acad. Sci. Ser. IV* **2001**, *2*, 803−815.

(59) David, F.; Leibler, S. Multicritical unbinding phenomena and nonlinear functional renormalization-group. *Phys. Rev. B* **1990**, *41*, 12926−12929.

(60) Elender, G.; Kühner, M.; Sackmann, E. Functionalisation of Si/SiO$_2$ and glass surfaces with ultrathin dextran films and deposition of lipid bilayers. *Biosens. Bioelectron.* **1996**, *11*, 565−577.